Defence Technology xxx (xxxx) xxx

Contents lists available at ScienceDirect

Defence Technology

journal homepage: www.keaipublishing.com/en/journals/defence-technology

# Influence of a liquid-filled compartment structure on the incoming shaped charge jet stability

X.D. Zu [a, b], Z.X. Huang [a, *], Z.W. Guan [b], X.C. Yin [c], Y.M. Zheng [a]

[a] School of Mechanical Engineering, Nanjing University of Science and Technology, Xiaolingwei 200, Nanjing 210094, China
[b] School of Engineering, University of Liverpool, Liverpool, L693GQ, UK
[c] Department of Mechanics and Engineering Science, Nanjing University of Science and Technology, Nanjing 210094, China

ARTICLE INFO

*Article history:*
Received 22 October 2019
Received in revised form
14 March 2020
Accepted 15 March 2020
Available online xxx

*Keywords:*
Compartment structure
Shaped charge jet
Shock wave
Disturbance
Stability

ABSTRACT

Liquid-filled compartment structure consists of a bulk steel plate with matrix blind holes which are filled with liquid and a steel front plate to seal up the liquid with rings and bolts. The liquid-filled compartment structure can resist the shaped charge warhead effectively. This paper presents experimental and theoretical investigations of the penetration ability of the residual shaped charge jet emerging from the liquid-filled compartment structure after the penetration process at different impact angles. On the basis of shock wave propagation theory, the influence of the liquid-filled compartment structure on jet stability is analysed. The interferences of the liquid backflow caused by a reflected shock wave and a back plate on jet stability under different impact angles are also examined. In addition, the range of the disturbed velocity segments of the jet at different impact angles and the penetration ability of the residual jet are obtained. A theoretical model is validated against the experimental penetration depths.

© 2020 China Ordnance Society. Production and hosting by Elsevier B.V. on behalf of KeAi Communications Co. This is an open access article under the CC BY-NC-ND license (http://creativecommons.org/licenses/by-nc-nd/4.0/).

## 1. Introduction

The protective ability of the armours of armoured vehicles requires further enhancement to protect the crew and important equipment inside. Increasing only the hardness and thickness of the armour steel outside the vehicles is often insufficient to safety protection requirements. Thus, additional armours are widely used to improve the protective ability. Such armours must be light and have low collateral damage potential, as well as provide additional functions [1]. Explosive reactive armour (ERA), ceramic composite armour, space armour and grating armour are widely used in tank vehicles. ERA and ceramic composite armour are additional armours that can be used with the main armour. ERA can protect the vehicle from shaped charge and kinetic warhead effects, the fly plates from the ERA and the shockwave produced by the detonating ERA may harm personnel or equipment. By contrast, ceramic composite armour can resist attack from a kinetic warhead but cannot resist the shaped charge warhead effectively [2].

A liquid-filled compartment structure can be used as additional armour [3]. One type of liquid-filled compartment structure consists of a bulk steel plate, which is drilled on matrix blind holes that can be linked together by small channels and liquid (e.g. water and diesel) that is injected in the hole, and a steel front plate to seal up the liquid with rings and bolts. The liquid volume in one blind hole is small, so even if the liquid is fuel, it is difficult to ignite. Liquid-filled compartment structure armour can provide effective protection against shaped charge warhead effectively and reduce the weight of additional armours [4,5]. The liquid can be used for other purposes, such as put out a fire when necessary. To date, limited studies (gauging from publications in open literature) have been conducted on the interaction mechanism between the liquid-filled compartment structure and shaped charge jet (SCJ).Held [6] introduced the effect process of water filled columns to the shaped charge jet. Based on the X-ray experiments he pointed that the stronger the radial confinement in the case of water, the more collapse effect is achieved. Fourest et al. [7,8] analysed the bubble dynamics through a hydrodynamics ram in a pool and liquid-filled container by using the Rayleigh–Plesset equation. The results show that the liquid compressibility effect influences the dynamics of confined bubbles, and the pressure of the gas in the bubble only slightly influence the bubble dynamics and hydrodynamic loads

* Corresponding author. School of Mechanical Engineering, Nanjing University of Science and Technology, Xiaolingwei 200, Nanjing 210094, China. .
*E-mail address:* huangyu@njust.edu.cn (Z.X. Huang).
Peer review under responsibility of China Ordnance Society

https://doi.org/10.1016/j.dt.2020.03.009
2214-9147/© 2020 China Ordnance Society. Production and hosting by Elsevier B.V. on behalf of KeAi Communications Co. This is an open access article under the CC BY-NC-ND license (http://creativecommons.org/licenses/by-nc-nd/4.0/).

Please cite this article as: Zu XD et al., Influence of a liquid-filled compartment structure on the incoming shaped charge jet stability, Defence Technology, https://doi.org/10.1016/j.dt.2020.03.009

**Nomenclature**

| | |
|---|---|
| $\rho$ | Density (kg/m3) |
| $c$ | Sound velocity (m/s) |
| $\sigma_s$ | Yield strength (MPa) |
| $\sigma_b$ | Tensile strength (MPa) |
| $e$ | Elongation (%) |
| $\theta$ | Impact angle (°) |
| $D_{wi}$ | Crater diameter of the witness target (mm) |
| $D_{ti}$ | Penetration crater diameter of the front plate of the liquid-filled compartment structure target (mm) |
| $D_{to}$ | Back crater diameter of the back plate of the liquid-filled compartment structure target (mm) |
| $l_j$ | Length of a SCJ when it penetrates the target (mm) |
| $C_j$ | Sound velocity of the SCJ material (m/s) |
| $v_j$ | Velocity of the jet tip (m/s) |
| $u$ | Penetration velocity (m/s) |
| $\rho_j$ | Density of the jet (kg/m$^3$) |
| $\rho_t$ | Density of the target (kg/m$^3$) |
| $2\alpha$ | Shockwave angle (°) |
| $P$ | Depth of penetration in the witness target (mm) |
| $C_l$ | Sound speed in the liquid (m/s) |
| $V_j$ | Shaped charge jet tip velocity (m/s) |
| $\gamma$ | Angle between incident shock wave and reflection shock wave (°) |
| $\Delta S$ | Distance of the jet segment to the compartment wall |
| $ds$ | Distance of the jet segment to the axis line of the compartment of the target |
| $S_1$ | Distance of the incident shock wave moving from shock wave front to the wall |
| $\tau$ | Time constant |
| $P_1$ | Incident shock wave intensity at the wall |
| $P_2$ | Reflection shock wave intensity at the wall |
| $S_2$ | Distance of the reflection shock wave moving from the wall to the axis of the jet |
| $P_3$ | Reflection shock wave intensity when it reaches the axis of the jet |
| $dm_j$ | Mass of the jet finite segment (kg) |
| $dS_l$ | Surface area of the jet element with the liquid finite segment (m$^2$) |
| $dv_r$ | Vertical drift velocity of the jet (m/s) |
| $r_c$ | Crater of the back plate penetrated by the jet (mm) |
| $R_t$ | Dynamic strength of the front plate material |
| $d_b$ | Diameter of the break jet (mm) |
| $t_b$ | Break time of SCJ (μs) |
| $\dot{\varepsilon}_b$ | Strain rate |
| $z_0$ | Distance from the virtual origin to the target |
| $t_0$ | Time when the first jet finite segment reaches the witness target |
| $\Delta V_{ji}$ | Velocity difference of the $i$th jet from head to tail |
| $l_{0i}$ | Length of the $i$th jet finite segment at the time $t_0$ |
| $l_i$ | Length of jet finite segment |
| $\Delta t_i$ | Penetration time for the $i$th jet finite segment |
| $\Delta P_i$ | Depth of penetration by the $i$th jet finite segment |
| $P_i$ | Total depth of penetration |
| $d_i$ | Diameter of the $i$th jet finite segment |

applied to the structure. Lecysyn [9] analysed the shock wave propagation, cavity formation and energy loss of fluid-filled tanks under a high-speed projectile impact through experimental work and theoretical modelling. The experimental phenomena can be described by the model. Disimile [10] explored a liquid spurt induced by the impact and penetration of a high-energy projectile into a liquid-filled tank through particle image velocimetry. Uhlig [11] examined the interplay between the eroded target material and the remaining projectile when copper rods perforated liquid-filled channels that were circumferentially confined by steel cylinders. The channel width plays a much more important role during penetration for a low-density material than for a high-density material. Lee [12] explored the penetration of jet particles using water through high-speed photography and X-ray experiments. The researchers found that the contour penetration cavities is not smoothly curved, but has a wavy structure. Also, the jet particles do not contribute to penetration of the liquid before foregoing particles are completely consumed. Held [14] modified the Szendrei equations and obtained the reaming equations of jet penetration in water through high spatial and temporal resolutions with the profile streak technology. On the basis of the virtual origin concept, Gao [4] established a mechanical model of a diesel oil-filled hermetic structure that interferes with a jet and obtained expressions for the affected velocity range of a jet. They also verified the theoretical model through X-ray experiments. In the theoretical model, the shock wave propagation path was simplified such that the shock wave movement path was normal in the axis of the SCJ, and the effect on the back plate to the jet was ignored. Zhang [5] considered that the spray of a liquid and radial direct convergence in the diesel oil-filled hermetic structure causes a SCJ to be unstable.

Although the mechanisms of the interaction of a single liquid-filled structure with a SCJ have been investigated for normal penetration, the mechanisms of a liquid-filled compartment structure with a SCJ under various impact angles have not yet been reported in open literature yet to the best of the authors' knowledge. In the current research, experimental results for the penetration of a liquid-filled compartment structures by the standard shaped charges under different impact angles are obtained and discussed. In addition, a theoretical model that takes into account the shock wave movement normal to the shock wave front and considers the effect of the back plate on the stability of the jet is established to explain the influence of the penetration process through the liquid-filled compartment structure on the shaped charge's residual penetration ability. The model can accurately calculate the disturbed jet velocity range and the depth of penetration of the residual jet into the witness target.

## 2. Experimental work

### 2.1. Liquid-filled compartment structure

A liquid-filled compartment structure consists of a main armour body and a front plate. The main armour body is composed of bulk 45# steel which is drilled with rectangular matrix blind holes that can be linked together by small channels, a seal ring groove and bolt holes that are machined on the edge of the main target body (Fig. 1). In this research, the materials of the main target body and the front plate are 45# and Q235 steels, respectively, and the liquid injected into the hole is diesel oil. Table 1 lists the material parameters. After the injection of diesel oil into the compartments, the front plate is used to seal the liquid with rings and bolts. The total mass of the compartments structures filled with diesel oil is about 7835 g, and the surface density of that is approximately 287.3 kg/m$^2$.

Please cite this article as: Zu XD et al., Influence of a liquid-filled compartment structure on the incoming shaped charge jet stability, Defence Technology, https://doi.org/10.1016/j.dt.2020.03.009

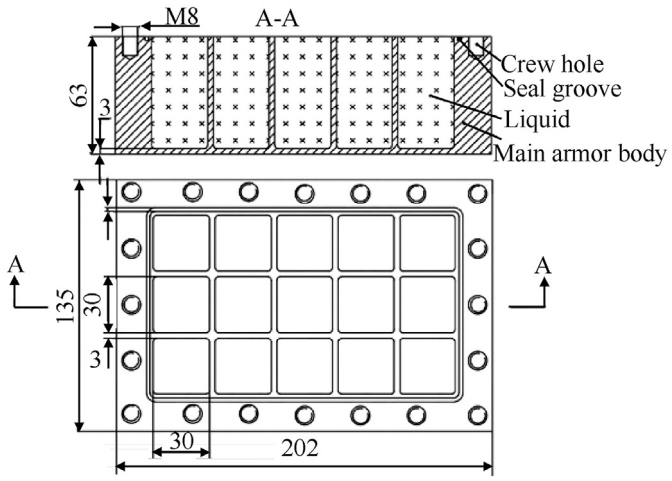


**Fig. 1.** Main target body (all dimensions in mm).

**Table 1**
Material parameters of the target.

| Material | $\rho$/(kg·m$^{-3}$) | $c$/(m·s$^{-1}$) | $\sigma_s$ /MPa | $\sigma_b$ /MPa | $e$ /% |
|---|---|---|---|---|---|
| 45# | 7850 | 5200 | 370 | 630 | 17 |
| Q235 | 7850 | 5200 | 235 | 375 | 26 |
| diesel oil | 873 | 1775 | – | – | – |

### 2.2. Standard shaped charge

For general research, a $\phi$56 mm standard shaped charge is adopted (Fig. 2). The standard shaped charge, with a respective weight and height of 180 g and 73.3 mm, has a 1-mm thick, oxygen-free, highly conductive copper cone liner and a JH-2 explosive with a density of 1.72 g/cm$^3$. The standard shaped charge is detonated by an 8# detonator. The depth of penetration is stable, with a depth variation of no more than 5%. The relationship between the penetration depth and standoff distance of the standard shaped charge is shown in Fig. 3. According to the experiments, the jet tip velocity is 6453 m/s, and that of the jet tail is 1179 m/s. The jet tip diameter is 2.5 mm, and the jet tail diameter is 13 mm. The jet tip starts to break at approximately 59 μs when the jet moves in the air. The length of the jet at 80 mm standoff is equal to 111.5 mm. The detailed parameters of the standard SCJ can be found in Ref. [16].

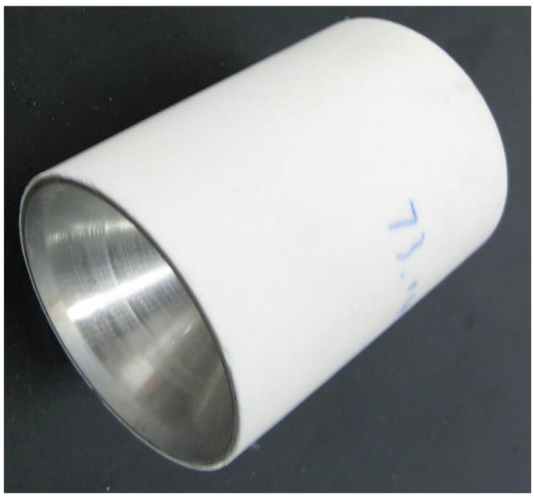

**Fig. 2.** Standard shaped charge.

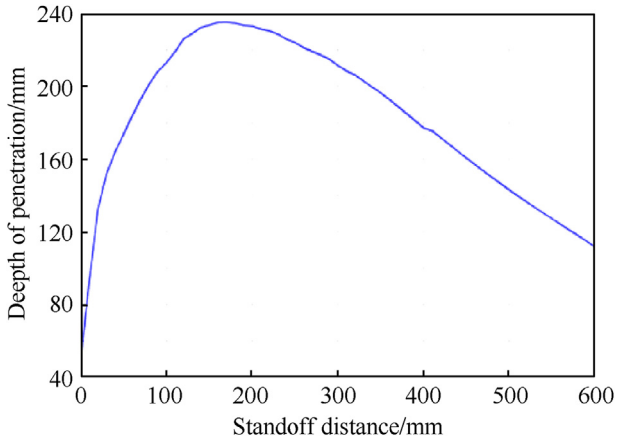


**Fig. 3.** Relationship between penetration depth and standoff distance of the standard shaped charge.

### 2.3. Experimental setup

The liquid-filled compartment structure target is placed on a steel target frame with a defined impact angle after the target is assembled. The standoff distance from the charge to the armour module is provided by a hollow polyethylene cylinder of which the centreline length is 80 mm. The impact angle θ is defined by the angle between the normal on the armour module and the shotline of the shaped charge jet. The standoff from the base of the shaped charge to the witness target is 330 mm. The arrangement of the shaped charge and target is shown in Fig. 4, and a real experimental setup is presented in Fig. 5.

### 2.4. Experimental results

The residual penetration and the crater diameters in the witness target, as well as that of both front and back plates of the armour module, was measured after each firing at different impact angles. This date is reported in Table 2 and graphically in Figs. 6 and 7.

Table 2 and Fig. 6 reveal that the crater diameters ($D_{ti}$ and $D_{to}$) on the liquid-filled compartment target increase but the crater diameter ($D_{wi}$) of the witness target decreases with the increase of the impact angle. The radial draft of the particulated jet elements increases with the impact angle. The depth of penetration into the witness target changes non-monotonically with the impact angle. The minimum penetration depth is obtained when the impact angle is at 0° (Fig. 7).

## 3. Theoretical model

### 3.1. Discerption of a shaped charge jet with a liquid-filled compartment target

The penetration velocity of a SCJ is faster than the sound speed through a liquid. The shock wave formed from the tip of a SCJ is illustrated in Fig. 8. The shock wave angle is denoted by $\alpha$. The density and temperature of the liquid increase behind the shock wave front, and a cavity area is formed between the SCJ and the shock wave front. The interaction time is very short. Thus, the temperature effect and vaporisation of the liquid are typically ignored.

The schematic of the break-up of the SCJ due to the liquid-filled

Please cite this article as: Zu XD et al., Influence of a liquid-filled compartment structure on the incoming shaped charge jet stability, Defence Technology, https://doi.org/10.1016/j.dt.2020.03.009

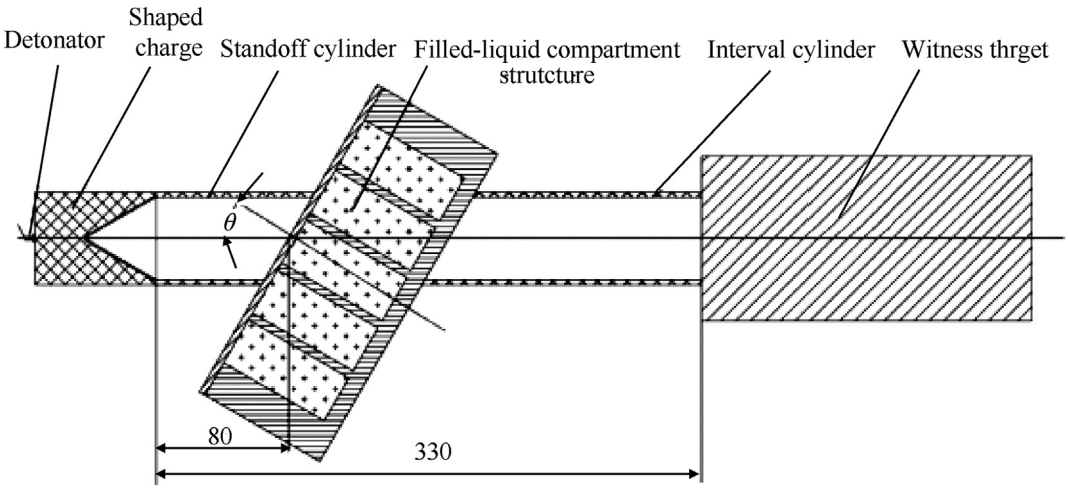


**Fig. 4.** Layout of the experiment (all dimensions in mm).

**Fig. 5.** Experimental setup.

**Table 2**
Experimental results.

| No. | $\theta$/° | $P$/mm | $D_{wi}$/mm | $D_{ti}$/mm | $D_{to}$/mm |
|---|---|---|---|---|---|
| 1 | 0 | 59 | 18 × 24 | 21 × 21 | 103 × 42 |
| 2 | 0 | 62 | 18.5 × 24.5 | 20 × 21 | 98 × 42 |
| 3 | 20 | 108 | 15 × 15 | 16.5 × 26 | 108 × 53 |
| 4 | 20 | 116 | 16 × 10 | 22 × 22 | 112 × 55 |
| 5 | 30 | 89 | 14 × 10 | 24 × 20 | 125 × 60 |
| 6 | 30 | 83 | 15 × 9.5 | 21 × 22 | 122 × 63 |
| 7 | 45 | 69 | 18 × 21 | 18 × 21 | 136 × 55 |
| 8 | 45 | 64 | 18 × 25 | 18.5 × 24 | 134 × 53 |
| 9 | 60 | 76 | 10 × 16 | 55 × 25 | 149 × 42 |
| 10 | 60 | 77 | 10 × 16 | 54 × 23 | 143 × 42 |

compartment target is depicted in Fig. 9. The incident shock wave formed by the SCJ runs through the liquid, and then the shock wave reflects at the compartment structure wall plate and forms a reflection shock wave. The stability of the SCJ is subjected to the reflected shock wave interaction with the penetration crater. Thus, after the reflection shock wave drives the liquid to move to the axis of the direction of the SCJ, the stability of this part of the jet is broken, creating finite segments with radial drift velocity or tumbling behavior. As the diameter of the holes on the back plate changes over time and the edge of the holes interacts with the jet intermittent, the stability of the SCJ can be similarly disturbed. The liquid-filled compartment structure disturbs the stability of the middle part of the SCJ.

### *3.2. Interaction between the shaped charge jet and the liquid-filled compartment structure target*

The interaction between the SCJ and the liquid-filled compartment structure target can be divided into four stages. In the first stage, the SCJ perforates the front plate in a steady-state penetration. In the second stage, the SCJ perforates the liquid inside the compartment structure. The shock wave moves to the direction normal to the wave front after the shock wave is formed as the jet penetrates the liquid. This incident shock wave is formed when the SCJ penetrates the liquid. The shock wave reflects at the compartment structure wall, and the reflection shock wave makes the liquid move in the direction of the axis of the shaped charge jet, thereby disturbing jet stability. When the compartment target is at an inclination angle, the SCJ may perforate more than one compartment. The process whereby the jet perforates the wall of a compartment can be considered a steady-state penetration. In the third stage, the SCJ perforates the back plate, and the jet is intermittently disturbed for a few times. In the final stage, the back part of the jet is not disturbed and goes through the liquid-filled compartment target. The residual jet penetrates the witness target.

### *3.3. Influence of the liquid inside the compartment structure on the shaped charge jet*

To derive the theoretical model, the following assumptions are made:

(1) The gravity effect is negligible.
(2) The thermal conductivity is ignored.

Please cite this article as: Zu XD et al., Influence of a liquid-filled compartment structure on the incoming shaped charge jet stability, Defence Technology, https://doi.org/10.1016/j.dt.2020.03.009

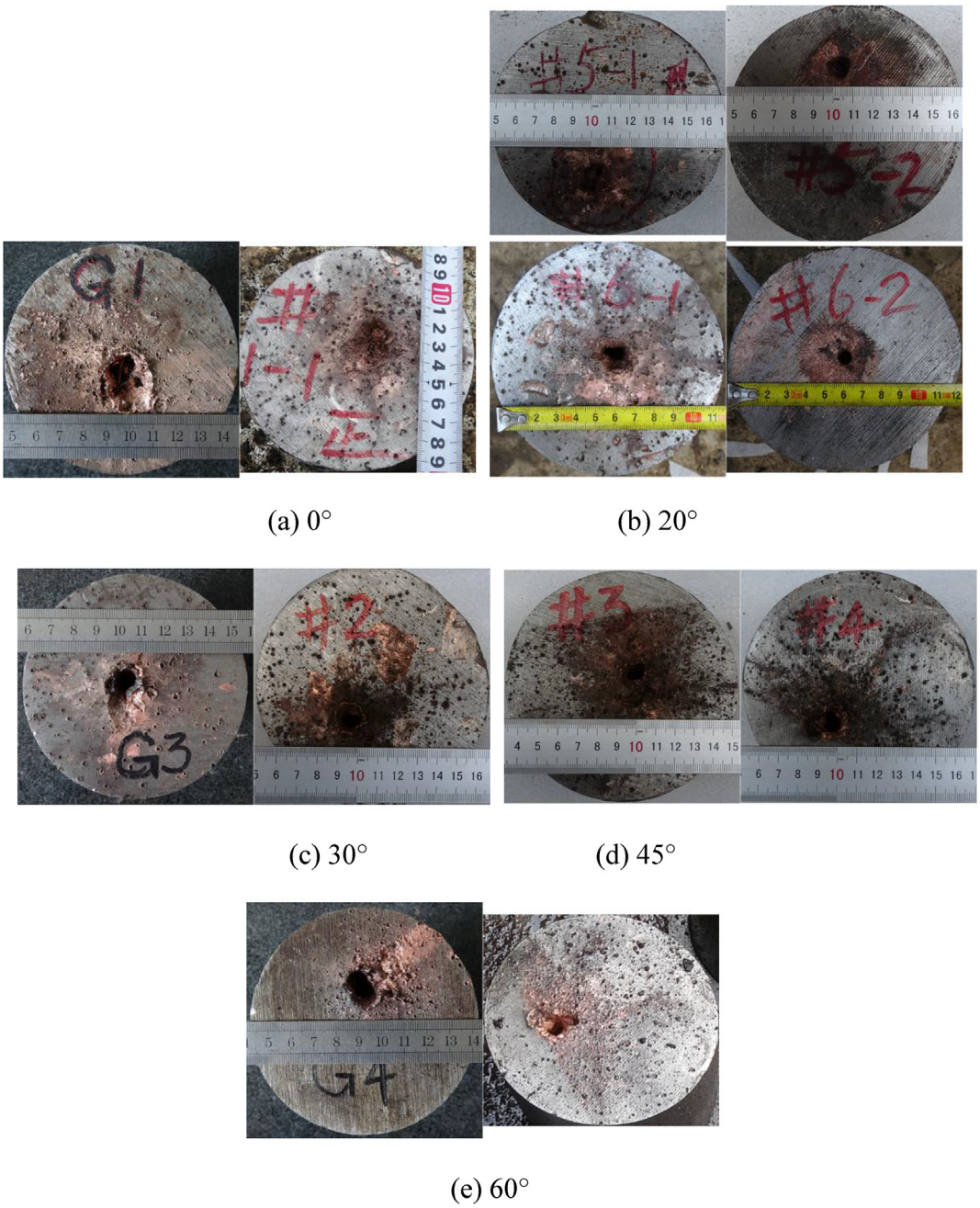


(a) 0° (b) 20°

(c) 30° (d) 45°

(e) 60°

**Fig. 6.** Crater on the witness targets under different impact angles.

(3) The density of the liquid and the sound speed of the liquid effects are ignored and considered constant.

The velocity of the penetrator will be reduced when the stress wave move in the penetrator a circle [13], which will causes several impacts on the liquid by the SCJ. The interval time between two impacts can be obtained as

$$\Delta t = \frac{2l_j}{C_j} \tag{1}$$

where $l_j$ is the length of the SCJ when it penetrates the target, and $C_j$ is the sound speed in the SCJ material.

The relationship between the velocity of the jet tip $v_j$ and penetration velocity $u$ is expressed as follows:

$$u = \frac{v_j}{1 + \sqrt{\rho_t/\rho_j}} \tag{2}$$

where $\rho_j$ is the density of the jet, and $\rho_t$ is the density of the target.

According to reference [14], the penetration pressure caused by a SCJ penetrating the target can be calculated as

$$P = \frac{1}{2}\rho_j (v_j - u)^2 \tag{3}$$

When the jet moves through the liquid, the half cone angle $(\alpha)$ of the shock wave (Mach wave) can be obtained as

Please cite this article as: Zu XD et al., Influence of a liquid-filled compartment structure on the incoming shaped charge jet stability, Defence Technology, https://doi.org/10.1016/j.dt.2020.03.009

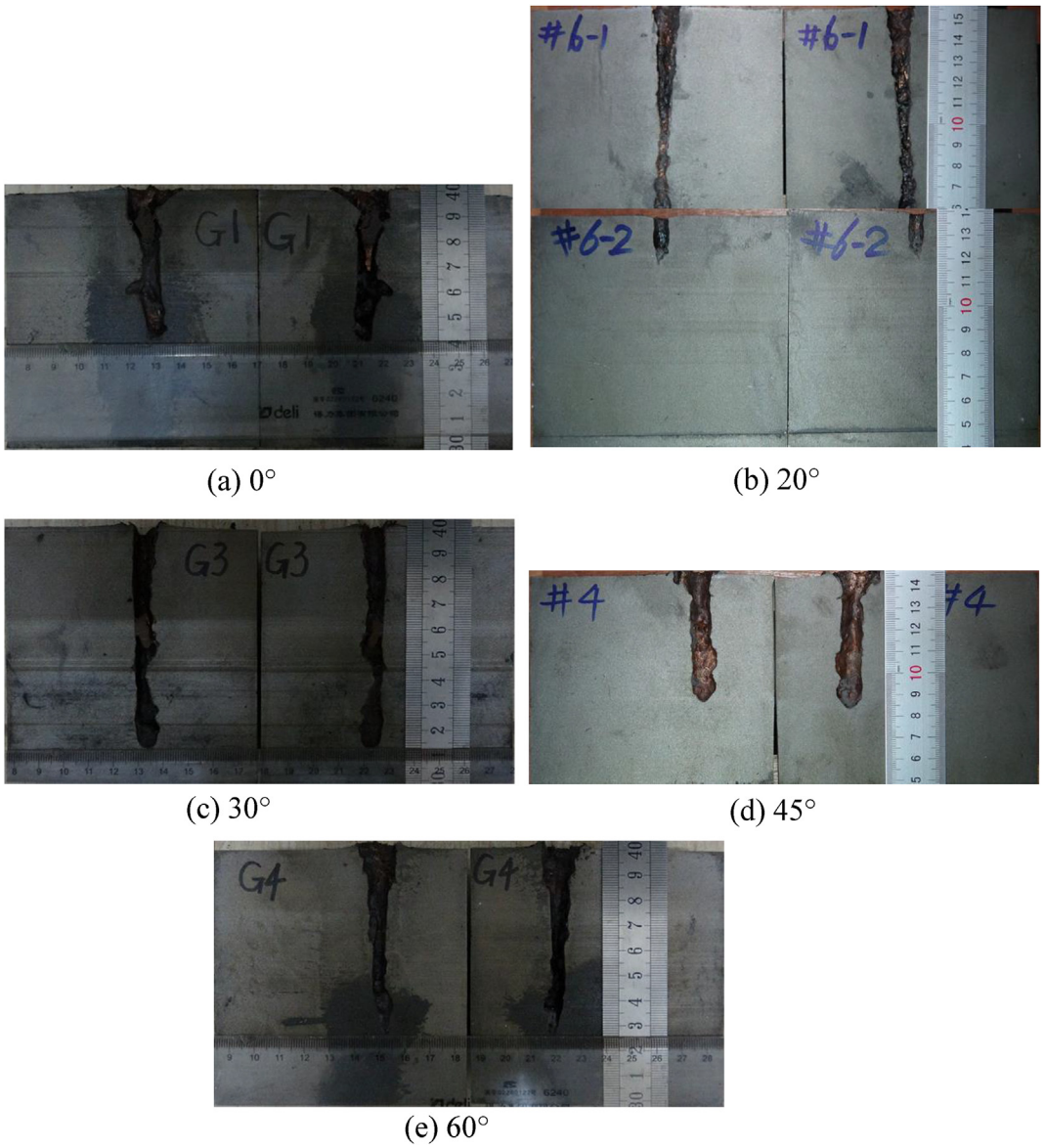


**Fig. 7.** Cut witness targets from experiments with different impact angles.

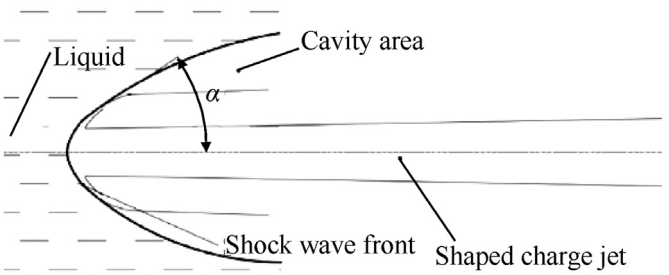


**Fig. 8.** Schematic of a shock wave generated by a SCJ.

$$\alpha = \arcsin\frac{C_l}{V_j} \tag{4}$$

where $C_l$ is the sound speed in the liquid, and $V_j$ is the SCJ's tip velocity.

A typical propagation path of a shock wave is illustrated in Fig. 10. If the path of the reflected shock wave is not across the penetration path, then the SCJ is considered undisturbed. The angles between the propagation and the normal direction of the liquid-filled compartment structure target, $\gamma_{1,2}$, can be calculated as follows:

$$\gamma_{1,2} = \theta \pm \alpha \tag{5}$$

To simplify the model, the SCJ is symmetric in the width of the armour module is considered. Based on Eq. (5), the distance of the incident shock wave moving in the compartment from the shock wave front to the compartment wall is expressed as follows:

$$S_1 = \Delta S/\cos(\alpha \pm \theta) \tag{6}$$

where ± depends on the shock wave translation direction.

The movement time of the incident shock wave is

Please cite this article as: Zu XD et al., Influence of a liquid-filled compartment structure on the incoming shaped charge jet stability, Defence Technology, https://doi.org/10.1016/j.dt.2020.03.009

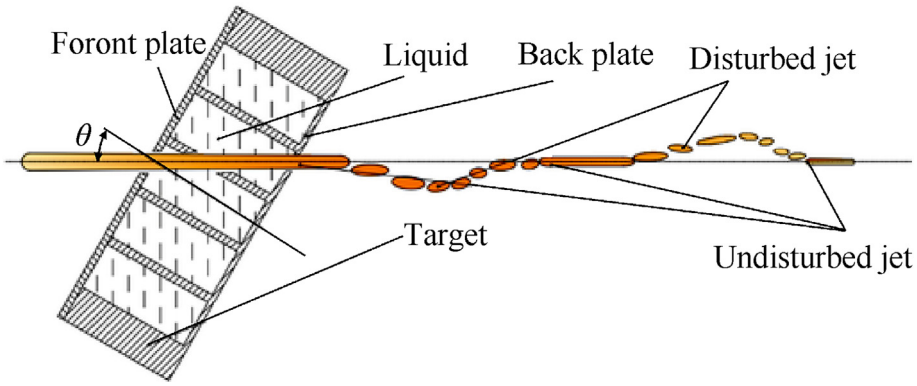


**Fig. 9.** Schematic of the break-up of the shaped charge jet due to a liquid-filled compartment target.

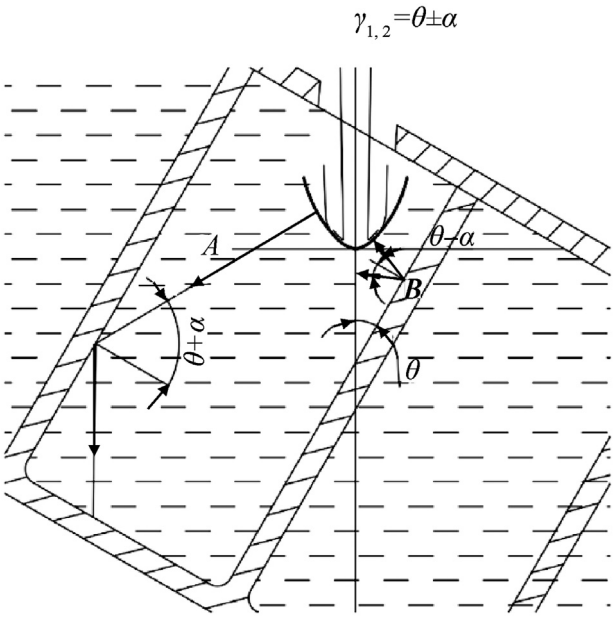


**Fig. 10.** Schematic of the propagation path of the shock wave.

$$\Delta t_1 = \frac{S_1}{C_l} \tag{7}$$

The shock wave intensity decays exponentially when it propagates through the liquid. Thus, when the shock wave reaches the wall of the compartment, its intensity is

$$P_1 = Pe^{-\frac{t}{\tau}} \tag{8}$$

where $\tau$ is a time constant.

The reflection coefficient [15] of the shock wave from the wall is

$$C_R = 0.0012P_1^5 - 0.0211P_1^4 + 0.1440P_1^3 - 0.14753P_1^2 + 0.7974P_1 + 1.9560 \tag{9}$$

Here, the unit of $P_1$ is GPa.

The reflection shock wave intensity is

$$P_2 = C_R P_1 \tag{10}$$

Based on the law of sines, the distance of the reflection shock wave before it meets the jet is

$$S_2 = \frac{S_1 \cos\alpha}{\cos(2\gamma - \alpha)} \tag{11}$$

The movement time of the reflection shock wave can then be expressed as

$$\Delta t_2 = \frac{S_2}{C_l} \tag{12}$$

The point that the shaped charge jet starts to penetrate the armour module is set as the coordinate origin (0, 0), and the time is defined as $t_0$. The direction that the axis of the shaped charge jet as the $X$ direction. If a shock wave formed at $t'$ and ($x'$, 0). Then the interaction location that the reflect shock wave with the shaped charge jet segment is $(x' + (S_1^2 + S_2^2 - 2S_1S_2\cos(2(\theta-\alpha)))^{1/2}, 0)$, and the interaction time is $(t' + t_1 + t_2)$. The shaped charge jet segment which move that location at the interaction time will be disturbed.

Based on Equations (8)–(11), the reflection shock wave intensity on the point where the liquid disturbs the jet finite segment is

$$P_3 = C_R P \cdot e^{-\frac{t_1+t_2}{\tau}} \tag{13}$$

The interaction between the jet and liquid finite segment is displayed in Fig. 11. The reflection shock wave makes the liquid finite segment move in the direction of the reflection shock wave. The velocity component in the vertical direction enables the jet finite segment to have a lateral drift velocity and flip turn. Basing on the momentum theorem and the conservation law of momentum, the lateral drift velocity of the jet finite segment can be obtained as

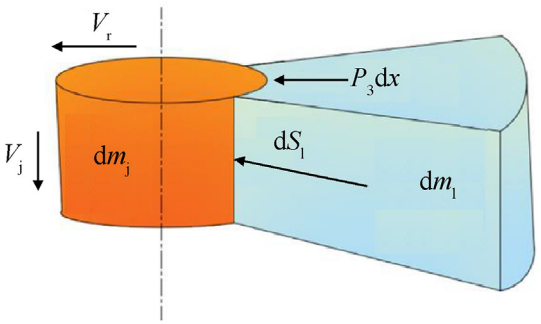


**Fig. 11.** Interaction between the jet and liquid finite segment.

Please cite this article as: Zu XD et al., Influence of a liquid-filled compartment structure on the incoming shaped charge jet stability, Defence Technology, https://doi.org/10.1016/j.dt.2020.03.009

$$\frac{dm_j}{dS_l}\cdot\frac{dv_r}{dt} = C_R P_3 \sin\left[\frac{\pi}{2}+\alpha-2(\alpha\pm\theta)\right] \tag{14}$$

where $dm_j$ is the mass of the jet finite segment, and $dS_l$ is the surface area of the jet element wetted by the liquid segment. Each finite segment can be seen as a small circular truncated cone. Therefore, $dm_j$ and $dS_l$ are the mass and cone surface area of the small circular truncated cone wetted by the liquid segment. $dv_r$ is the lateral drift velocity of the jet.

### 3.4. Influence of the back plate on the shaped charge jet stability

The schematic of the back plate disturbing the stability of the SCJ is shown in Fig. 12.

Fig. 12 shows the movement sketch of the part on the back plate near the crater, and part of the SCJ is disturbed. The edge point on the expanding hole of the back plate moves under the jet, expanding the crater force and the liquid in the compartment to the back plate. When the crater expanding the edge of the crater can reach the SCJ moving path several times and disturb the stability of the jet.

When the SCJ perforates the liquid-filled compartment structure, the front plate usually cannot disturb the stability of the SCJ. However, the crater on the back plate enlarges and disturbs the stability. According to Ref. [17], the crater of the back plate changes as follows:

$$r_c = \sqrt{A\Big/B-\left(\sqrt{A\Big/B-r_j^2}-\sqrt{Bt}\right)^2} \tag{15}$$

$$A = \frac{r_j^2 v_j^2}{\left(1+\frac{\rho_t}{\rho_j}\right)^2} \tag{16}$$

$$B = \frac{2R_t}{\rho_t} \tag{17}$$

where $t$ is the time measurement of expansion of the penetration hole on the back plate. When $t = t_f$ (the time corresponding to the ultimate expansion), the penetration hole is the largest, and the diameter of the crater hole cannot increase further. $t_f$ may be expressed as follows:

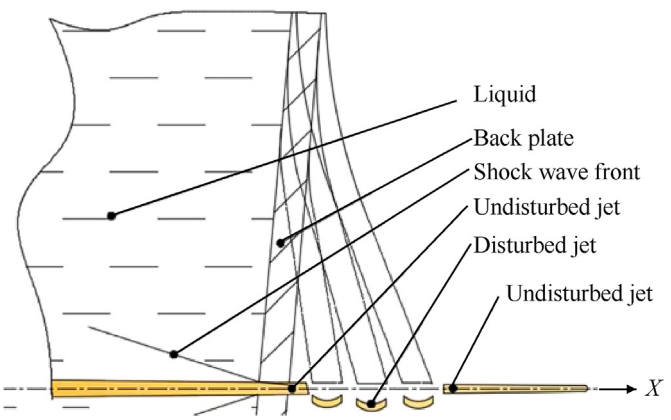


**Fig. 12.** Schematic of back plate disturb the stability of the jet.

$$t_f = \sqrt{A\Big/B-r_j^2}\Big/\sqrt{B} \tag{18}$$

To simplify the model of the back plate that disturbs the SCJ, the following assumptions are made: (1) the jet velocity during the perforation of the back plate is constant and (2) one finite segment of the jet cannot be disturbed by the neighbouring finite segment.

The perforation velocity when the SCJ perforates the liquid in the liquid-filled compartment structure target can then be calculated using Eq (2). A Cartesian coordinate system is established here, i.e. denoting the direction of the jet velocity as the x-direction, and the direction perpendicular to the jet velocity as the y-direction. Considering the effect of the shock wave projection coefficient, the movement track of an edge point on the expanding hole of the back plate is

$$\begin{cases} x = C_T u\sin(\alpha-\theta)t \\ y = C_T u\cos(\alpha-\theta)t + r_c t \end{cases} \tag{19}$$

where $C_T = \frac{2\rho_t C_t}{\rho_t C_t+\rho_l C_l}$.

The substitution of Eq. (15) into Eq. (19) yields

$$y = x\ \mathrm{ctg}(\alpha-\theta) + \sqrt{A\Big/B-\left(\sqrt{A\Big/B-r_j^2}-\sqrt{B}\times\frac{x}{C_T u\sin(\alpha-\theta)}\right)^2} \tag{20}$$

When $y$ is 0, the distance at the crater edge between the contacts with the SCJ from the location to the next location can be expressed as

$$x = \frac{\sqrt{A\Big/B-r_j^2}\pm\sqrt{A+\left[C_T u v_j\sin(\alpha-\theta)\right]^2}\times C_T u v_j\cos(\alpha-\theta)}{B+\left[C_T u v_j\sin(\alpha-\theta)\right]^2} \tag{21}$$

The direction of $x$ agrees with the direction of $C_T u v_j\sin(\alpha-\theta)$. Thus, the '+' marked in Eq. (21) is selected, and the interval of the back-plate interference on the SCJ is written as

$$x = \frac{\sqrt{A\Big/B-r_j^2}+\sqrt{A+\left[C_T u v_j\sin(\alpha-\theta)\right]^2}\times C_T u v_j\cos(\alpha-\theta)}{B+\left[C_T u v_j\sin(\alpha-\theta)\right]^2} \tag{22}$$

To simplify the calculations, the length of the disturbed SCJ is considered as the thickness of the back plate.

### 3.5. Theoretical model of the lateral drift velocity of the jet

The theoretical model of the lateral drift velocity of the jet indicates that the depth of penetration of the SCJ changes with the stand-off distance. According to the latent manufacturing imperfections of the liner, the strain rate of the liner material and the diameter of the jet when it breaks up, jets have a consistently low drift velocity after formation. If no external interference occurs, then the status of the material and the processing technology are confirmed, then the drift velocity of the jet is

$$v_d = \xi d_b \dot{\varepsilon}_b \tag{23}$$

where $\xi$ is a constant related to the material state and processing technology. The strain rate of the jet equals the velocity gradient

Please cite this article as: Zu XD et al., Influence of a liquid-filled compartment structure on the incoming shaped charge jet stability, Defence Technology, https://doi.org/10.1016/j.dt.2020.03.009

over the unit length of the jet. Then, $\dot{\varepsilon} = \mathrm{d}V/\mathrm{d}l$, where dV is the velocity gradient between two adjacent jet finite segments, and d$l$ is the length between them. Based on the virtual origin of the jet, the length of the jet finite segment is $\mathrm{d}l_\mathrm{b} = \mathrm{d}V \cdot t_\mathrm{b}$; thus, the strain rate when the jet breaks up, $\dot{\varepsilon}_\mathrm{b}$, is expressed as

$$\dot{\varepsilon}_\mathrm{b} = \frac{\mathrm{d}V}{\mathrm{d}l_\mathrm{b}} = \frac{1}{t_\mathrm{b}} \tag{24}$$

The lateral drift velocity [18] is

$$v_\mathrm{d} = \xi \frac{d_\mathrm{b}}{t_\mathrm{b}} \tag{25}$$

where $v_\mathrm{d}$ is the drift velocity without considering the external interference factor. With the SCJ penetrating the liquid-filled compartment structure target, the liquid in the compartment generates a back flow due to the action of the reflection shock wave which generates a lateral force. Thus, the jet finite segment obtains a certain lateral velocity $v_\mathrm{r}$. The liquid will have an asymmetric lateral force effect on the jet to exert an angular deviation in the jet motion, thereby resulting in a certain lateral velocity ($v_\theta$). Therefore, the lateral drift velocity of the jet finite segment is expressed as

$$\begin{cases} v_\mathrm{c} = v_\mathrm{r} + v_\theta & 0 < t < t_\mathrm{b} \\ v_\mathrm{c} = v_\mathrm{d} + v_\mathrm{r} + v_\theta & t \geq t_\mathrm{b} \end{cases} \tag{26}$$

Assuming that the jet virtual origin coordinates are $(\overline{o}, \overline{t})$, the jet is divided into n finite segments. Furthermore, the velocity of the $i$th finite segment is $V_{ji}$, and the stand-off distance is $z_0$ (from the virtual origin to the target). Thus, the time when the first jet finite segment reaches the witness target is

$$t_0 = \frac{z_0}{V_{j1}} \tag{27}$$

Given the velocity difference of the $i$th jet from head to tail ($\Delta V_{ji}$), the length of this jet finite segment at time $t_0$ is

$$l_{0i} = \Delta V_{ji} \cdot (t_0 - \overline{t}) \tag{28}$$

If the total depth of penetration is $P_{i-1}$ before the $i$th jet finite segment reaches the target, then the time for the jet finite segment to hit the target is expressed as

$$t_i = \frac{P_{i-1} + z_0}{V_{ji}}. \tag{29}$$

Basing on the modified Bernoulli equation, the penetration velocity in the witness target of the $i$th finite segment can be written as

$$U_i = \frac{V_{ji} - \sqrt{\frac{\rho_t}{\rho_j} V_{ji}^2 + \left(1 - \frac{\rho_t}{\rho_j}\right) \frac{2R_t}{\rho_j}}}{1 - \frac{\rho_t}{\rho_j}} \tag{30}$$

The diameter of the hole created by the jet that penetrates the target [17] is

$$d_{ci} = \sqrt{\frac{A}{B}} \tag{31}$$

If the $i$th jet finite segment penetrates the liquid-filled compartment structure target without interference and time $t_i$ is less than break up time $t_\mathrm{b}$, then the jet does not break up during penetration. Thus, the jet finite segment length is described as

$$l_i = \Delta V_{ji} \cdot (t_i - \overline{t}) \tag{32}$$

The penetration time for the $i$th jet finite segment is

$$\Delta t_i = \frac{l_i}{V_{ji} - U_i} \tag{33}$$

The depth of penetration by this jet finite segment is

$$\Delta P_i = U_i \Delta t_i \tag{34}$$

After the penetration process by the $i$th jet finite segment is finished, the total depth of penetration is

$$P_i = \Delta P_{i-1} + \Delta P_i \tag{35}$$

Based on the volume constant, the diameter of the $i$th jet finite segment can be obtained as

$$d_i = \sqrt{\frac{d_{0i}^2 l_{0i}}{l_i}} \tag{36}$$

If the time $t_i$ of the $i$th jet finite segment is greater than break up time $t_\mathrm{b}$ or if this jet finite segment gains a lateral velocity when it passes through the liquid-filled compartment structure target and breaks up, then the $i$th jet finite segment proceeds off the axis before it reaches the bottom of the penetration hole. Thus,

$$v_\mathrm{c}(t_i - t_\mathrm{b}) > (d_{ci} - d_i)/2 \tag{37}$$

This jet finite segment cannot reach the bottom of the penetration hole to penetrate the target effectively. Thus,

$$\Delta P_i = 0$$

if

$$v_\mathrm{c}(t_i - t_\mathrm{b}) < (d_{ci} - d_i)/2 \tag{38}$$

The finite segment deepens the bottom of the penetration hole. The depth of penetration is calculated using Eq. (34), and the total depth of penetration is calculated using Eq. (35).

## 4. Theoretical results and discussion

Based on the theoretical model, the initial penetration point is assumed as the centre point of the compartment unit. Here, the time for the SCJ to initiate penetrating the target is set as 0, and the coordinate of the x-axis (the direction of the jet axis) is also set as 0. The penetration channel geometry of the liquid-filled compartment structure at different impact angles is shown in Fig. 13.

In Fig. 14, the disturbed time refers to the time after the SCJ starts to penetrate the liquid-filled compartment structure. The blue bar in the figure means that at the corresponding angle, the SCJ penetrates the junction region of the wall of the compartment and the back plate. At the junction region, the back plate cannot be seen as a thick plate, so no disturbance of the back plate to the jet exists. Fig. 14 shows that the disturbed time of the back plate increases with the impact angle. When the impact angle of the liquid-filled compartment structure target exceeds 16°, the edge point on the expanding hole of the back plate could not touch the SCJ anymore. Thus, the back plate no longer disturbs the stability of the jet.

The disturbed time of the jet and the disturbed location at the compartments at different impact angles are presented in Fig. 15. This figure exhibits that the starting disturbed time and location decrease with the increasing the impact angle from 0° to 15°. Furthermore, the disturbed time interval decreases with the

Please cite this article as: Zu XD et al., Influence of a liquid-filled compartment structure on the incoming shaped charge jet stability, Defence Technology, https://doi.org/10.1016/j.dt.2020.03.009

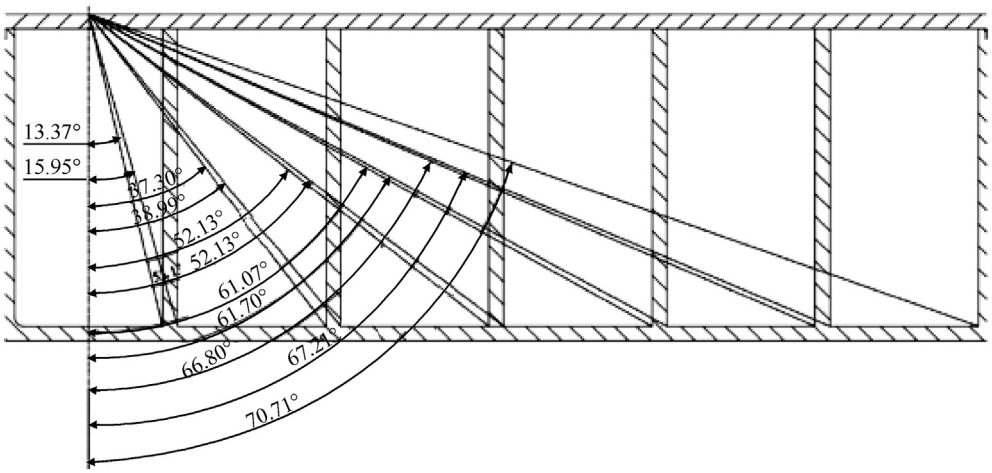


**Fig. 13.** Penetration channel geometry of the shaped charge jet under different impact angles.

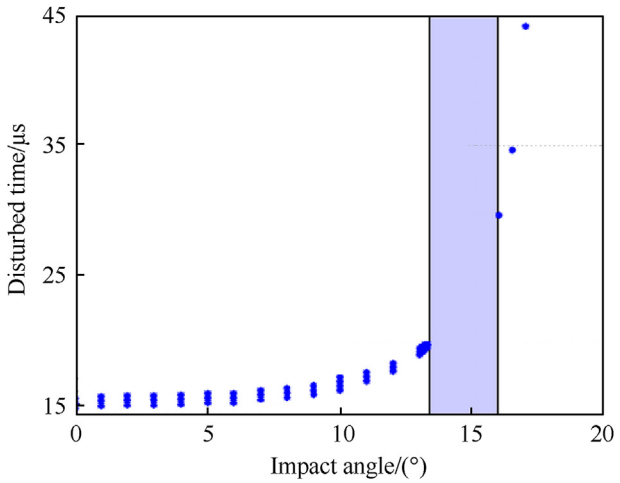


**Fig. 14.** Disturbed time of the SCJ by the back plate.

increase of the impact angle from 2° to 15°. The disturbed time interval and length decrease when the impact angle increases from 15.95° to 18.7°. Furthermore, when the impact angle exceeds 18.7°, the water in the liquid-filled compartment structure cannot disturb the stability of the SCJ.

Considering impact angle $\theta$ and half cone angle $\alpha$, the movement distance of the shock wave $(S_1 + S_2)$ decrease with the increasing impact angle, decreasing the disturbed time and the initial disturbed location. However, when the impact angle exceeds 13.37°, only the reflection shock wave at the right part of the SCJ can disturb the SCJ. The length of the wall of the compartment that can reflect the shock wave to disturb the jet decreases with the increasing impact angle. When the impact angle reaches 15.95°, the initial disturbed time is short, and the length of the wall of the compartment that can reflect the shock wave decrease obviously. When the impact angle exceeds 18.7°, the reflected shock wave does not penetrate the SCJ, so no disturbance exists from the compartment to the jet.

The disturbed velocity interval under different impact angles are demonstrated in Fig. 16. When the impact angle is less than 15°, the jet penetration channel is found in a compartment. When the impact angle increases, the angle between the jet velocity direction and the reflected shock wave direction $(\gamma)$ decreases (Fig. 10). Moreover, the time for the shock wave to generate the reflected one that reaches the jet penetration channel is reduced. Therefore, the distance from the shock wave to generate the location of the disturbed jet is shortened. When the impact angle is between

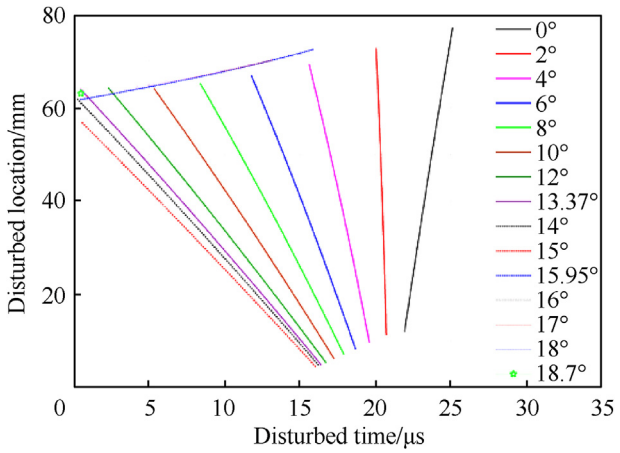


**Fig. 15.** Relationship between the disturbed time of the jet and disturbed location at the compartments under different impact angles.

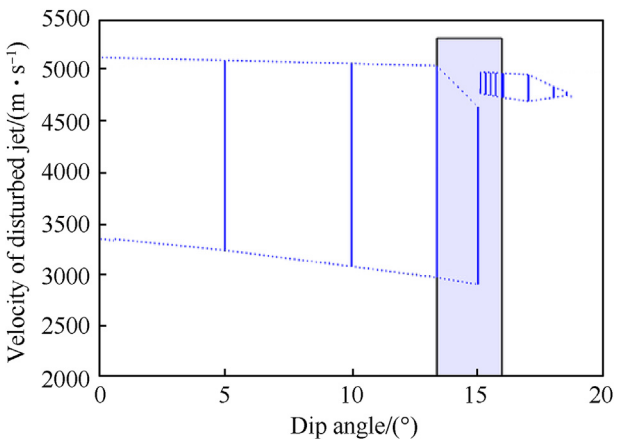


**Fig. 16.** Disturbed velocity interval of the shaped charge jet by the liquid-filled compartment structure target under different impact angles.

Please cite this article as: Zu XD et al., Influence of a liquid-filled compartment structure on the incoming shaped charge jet stability, Defence Technology, https://doi.org/10.1016/j.dt.2020.03.009

15.95° and 18.7°, the SCJ penetrates two compartments. When the impact angle of the target increases, the difficulty for the reflected shock wave to cross the jet penetration channel and disturb the stability of the jet increases.

Fig. 16 also depicts the stability of the SCJ disturbed by the backflow of the liquid-filled compartment structure and the back plate of the structure based on the results of Figs. 14 and 15. The disturbed velocity interval expands when the jet penetrates only one compartment. With the increase in the impact angle in the liquid-filled compartment structure, the disturbed velocity interval of the jet rapidly decreases when the jet penetrates two compartments. When the impact angle exceeds 18.7°, the liquid backflow and back plate deformation in the liquid-filled compartment structure offer no disturbance on the jet stability.

The penetration depth of the jet under different impact angles is shown in Fig. 17. This figure exhibits that the liquid-filled compartment structure target can interfere effectively with the stability of the jet and reduce its penetration capability, thereby increasing the protection capability of armoured vehicles. The theoretical calculation results of this research are consistent with the experimental results, as indicated in Fig. 17.

When the impact angle increases, the protective ability of the liquid-filled compartment structure target does not increase. Within the impact angle range of 0°–70°, the depth of penetration for the jet through the liquid-filled compartment structure is the smallest at approximately 15° and the largest near 18°. The main reasons for these results can be seen in Figs. 14–17. At 15°, the disturbed jet velocity range is large, and when the shaped charge jet penetrates the compartment, more steel wall of the compartment must be pierced than when the impact angle is lower than 13.37. When the impact angle is within 15.95°–18.7°, the disturbed jet velocity range decreases rapidly, sharply decreasing the penetration depth of the witness.

The penetration path extends with the increase in impact angle. However, shock wave angle $\alpha$ decreases with the velocity of the jet finite segment.

If the penetration point of the jet is at the centre of the first compartment, then the angle between the incident shock wave and the normal direction of a compartment wall that can disturb the jet is $\gamma = \alpha - \theta$ according to the theoretical analysis. When $\gamma > 0$, the backflow liquid which results in the reflected shock wave can disturb the stability of the SCJ.

This research shows that when the impact angle of the liquid-filled compartment structure exceeds 18.7°, the liquid backflow caused by the reflected shock wave will no longer disturb the jet stability.

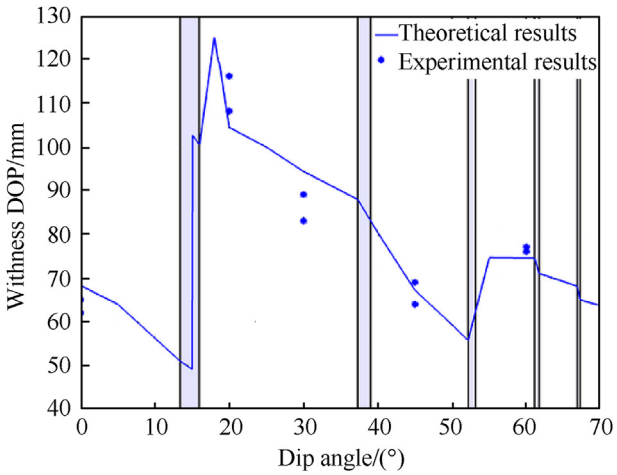


**Fig. 17.** Depth of penetration of the witness with different impact angles.

## 5. Conclusions

In the present research, the theoretical model is simplified to a 2D model, the penetration path of the SCJ passes through the axial plane of the compartment structure, and the effects of a corner or the second wall next to the corner of the compartment to the jet are ignored.

The liquid-filled compartment structure can disturb the stability of a penetrating jet effectively and reduce the penetration capability of the jet. However, the protective ability of the liquid-filled compartment structure does not increase with the impact angle.

The protective ability of the liquid-filled compartment structure mainly depends on the impact angle of the target, jet velocity and compartment size. The three parameters determine the distance of the motion path of the shock wave and disturbed ability of the compartments to the jet.

The disturbed jet velocity range is the greatest when the jet penetrates a channel in a single compartment. When the impact angle of the liquid-filled compartment structure exceeds the shock angle caused by the jet that penetrates the liquid in one compartment of the structure, the liquid backflow caused by the reflected shock wave no longer interferes with the stability of the jet.

When the impact angle of the liquid-filled compartment structure exceeds 16°, the deformation of the back plate no longer interferes with the stability of the jet.

By designing the size and direction of the compartment, the protective capability of the fuel tank can be effectively enhanced when penetrated by a high-speed SCJ.

## Declaration of competing interest

The authors declare that they have no known competing financial interests or personal relationships that could have appeared to influence the work reported in this paper.

## Acknowledgements

This research was supported by the National Natural Science Foundation of China (Grant No. 11472115, 11872214) and the China Scholarship Council (201706845026).

## References

[1] Mayseless M. Effectiveness of explosive reactive armor. J Appl Mech 2011;78(5):051006.
[2] Gooch W. An overview of protection technology for ground and space applications. Canberra, Australia: Second Australian Congress on Applied Mechanics; 1999. p. 10–2.
[3] Held Manfred Dipl Phys DR (DE). Wall for protection against shaped charges and kinetic-energy projectiles DEUTSCHE AEROSPACE AG, 80804 MUENCHEN. 1994. DE DE3122367, http://www.freepatentsonline.com/DE3122367.html.
[4] Gao Zhen-Yu, Huang Zheng-Xiang, Guo Min, et al. Theoretical study of a diesel-filled airtight structure unit subjected to shaped charge jet impact. Propellants, Explos Pyrotech 2016;41:62–8.
[5] Zhang X, Zu XD, et al. Analysis of liquid-filled unit holes structure subjected to shaped charge jet impact. Explos Shock Wave 2017;37(6):1101–6.
[6] Held M. Armour: 14th international symposium on ballistics, Quebec, Canada, 26-29 September 1993; proceedings, vol. 1. Messerschmitt-Bölkow-Blohm; 1993.
[7] Fourest T, Laurens JM, Deletombe E, et al. Analysis of bubbles dynamics created by hydrodynamic ram in confined geometries using the Rayleigh–Plesset equation. Int J Impact Eng 2014;73:66–74.
[8] Fourest T, Laurens JM, Deletombe E, et al. Cross validation of analytical and finite element models for Hydrodynamic Ram loads prediction in thin walled liquid filled containers. J Fluid Struct 2015;59:285–96.
[9] Lecysyn N, Bony-Dandrieux A, Aprin L, et al. Experimental study of hydraulic ram effects on a liquid storage tank: analysis of overpressure and cavitation

ARTICLE IN PRESS



induced by a high-speed projectile. J Hazard Mater 2010;178(1–3):635–43.
[10] Disimile PJ, Toy N. Liquid spurt caused by hydrodynamic ram. Int J Impact Eng 2015;75:65–74.
[11] Uhlig WC, Coppinger MJ. Hydrocode simulations of liquid filled channels for understanding erosion in shaped charge jet penetration. Proc Eng 2017;204:231–8.
[12] Lee ES, Oh KH, Song SY. Penetration of particulated shaped-charge jet into water. In: High-Speed photography and photonics: international congress. International Society for Optics and Photonics; 1995. p. 975–81.
[13] Rosenberg Z, Dekel E. Terminal ballistics. Berlin: Springer; 2012.
[14] Held M, Huang NS, Jiang D, et al. Determination of the crater radius as a function of time of a shape charge jet that penetrates water. Propellants, Explos Pyrotech 1996;21:64–9.
[15] Luo ZL, Zhou ZT, Mao HB. Theoretical analysis of the interaction between the plate structure and strong shock wave in underwater explosion. Chin J High Press Phys 2017;31(4):443–52.
[16] Xiao QQ, Huang ZX, Zu XD, et al. Influence of drift velocity and distance between jet particles on the penetration depth of shaped charges. Propellants, Explos Pyrotech 2016;41(1):76–83.
[17] Ru-jiang Li, Zhao-wu Shen. Effect of NATO angle and plate velocity on disturbance frequency of reactive armor against shaped charge jet. Chinese Journal of Energetic Materials 2008;16(3):295–7. 318.
[18] Segletes SB. Drift velocity computations for shaped-charge jets. Army Ballistic Research Lab Aberdeen Proving Ground MD; 1983.

Please cite this article as: Zu XD et al., Influence of a liquid-filled compartment structure on the incoming shaped charge jet stability, Defence Technology, https://doi.org/10.1016/j.dt.2020.03.009